Nanoscale Advances

ROYAL SOCIETY OF CHEMISTRY

PAPER

View Article Online
View Journal | View Issue

Cite this: *Nanoscale Adv.*, 2023, **5**, 160

A nanofiber hydrogel derived entirely from ocean biomass for wound healing†

Tian-Cai Sun,[a] Bing-Yu Yan,[a] Xu-Chao Ning,[b] Zhi-Yue Tang,[a] Chao Hui,[a] Mao-zhi Hu,[c] Seeram Ramakrishna,[d] Yun-Ze Long *[a] and Jun Zhang*[a]

Crustaceans and fish scales in the marine food industry are basically thrown away as waste. This not only wastes resources but also causes environmental pollution. While reducing pollution and waste, biological activity and storage of materials are urgent issues to be solved. In this study, by first preparing dry fibers and then making hydrogels, we prepared a fish scale/sodium alginate/chitosan nanofiber hydrogel (FS-P) by cross-linking the nanofibers *in situ*. From fish and other organisms, fish gelatin (FG), collagen and $CaCO_3$ were extracted. Fish scale (FS)/sodium alginate/chitosan nanofibers were cross-linked with copper sulfide nanoparticles prepared by a one-step green method to obtain FS-P nanofiber hydrogels under mild conditions without catalyst and additional procedures. These fiber hydrogels not only have good tissue adhesion and tensile properties, but also have the antibacterial effect of natural antibacterial and CuS photothermal synergism, which can achieve 51.32% and 49.96% of the antibacterial effect against *Staphylococcus aureus* and *Escherichia coli* respectively, avoiding the generation of superbacteria. The nanofiber hydrogels have 87.56% voidage and 52.68% degradability after 14 days. The combined strategy of using marine bio-based fibers to prepare gels promoted angiogenesis and tissue repair.

Received 10th August 2022
Accepted 20th October 2022

DOI: 10.1039/d2na00535b

rsc.li/nanoscale-advances

1 Introduction

At present, in most marine food production processes, crustaceans, fish scales, and so on[1] are basically thrown away as waste.[2,3] This not only wastes resources but even causes environmental pollution.[4,5] Materials and valuable applications beneficial to mankind can be obtained from these marine biological wastes.[6–9] For example, collagen can be extracted from fish and other organisms, sodium alginate can be extracted from sea algae, and chitosan can be extracted from crustaceans.[10–12] Recently, there have been extensive studies on these raw materials because of their excellent biocompatibility and biodegradability.[13] However, on the premise of reducing waste, there is still a lack of research on one-step green methods to extract and synthesize hydrogel excipients from marine waste.

Since fish scales and crustaceans are rich in polysaccharide macromolecules, collagen, amino acids and calcium carbonate have been isolated in various ways.[14] Amino acid gels, protoproteins, sodium alginate and chitosan are used as hydrogels.[15–17] More importantly, amino acids and collagen are highly bioactive, so they have been widely used in the management of severe wound healing.[18–22] They stimulate wound healing by promoting cell proliferation and differentiation.[23–25] Calcium carbonate and chitosan speed up blood clotting and blood vessel formation and maturation.[26] At present, collagen and other proteins used in clinical practice are mainly derived from readily available terrestrial organisms.[27,28] However, the increasing frequency of dangerous infectious diseases in terrestrial organisms has led us to worry about the health of animal extracts such as those from sheep, cattle and horses. Also, because marine waste is often discarded, environmental pollution and other problems result. Fish scales, for example, are considered inedible waste and make up about 3% of the total weight of fish; the transition of crustaceans prevents ecological imbalance.[29] Therefore, there is an urgent need to obtain new isolates from marine biological waste for medical research under cost-effective and sustainable conditions.[30] In addition, wound dressings in the field of biodegradable medical scaffolds can be prepared by microfluidic methods,[31] electrostatic spinning,[32] and polymer synthesis,[33–35] and by using hydrogel and other biomaterials.[36–39] As a flexible body, hydrogel has special advantages in the field of wound repair and other medical scaffolds: it keeps the wound moist, protects the wound from dehydration, absorbs additional secretions, allows gas

[a]*Collaborative Innovation Center for Nanomaterials & Devices, College of Physics, Qingdao University, Qingdao 266071, P. R. China. E-mail: yunze.long@qdu.edu.cn; iamjunzhang@163.com*

[b]*Medical College, Qingdao University, Qingdao 266071, P. R. China*

[c]*Equipment Division, Qingyun County People's Hospital, Dezhou 253000, P. R. China*

[d]*Center for Nanofibers & Nanotechnology, Department of Mechanical Engineering, National University of Singapore, Singapore 117574, Singapore*

† Electronic supplementary information (ESI) available. See DOI: https://doi.org/10.1039/d2na00535b

exchange, and is easy to remove without damaging the wound bed.[40] It has been widely used in the management of serious wound healing. However, the preservation environment of moist hydrogels is relatively special, and generally requires freeze-drying or low-temperature preservation, and may even cause deterioration. Ensuring the long-term viability of hydrogels is currently a challenge.[34,41,42] It is possible to solve this problem by restricting the precursors of the coated fiber membrane by electrostatic spinning and crosslinking the fiber membrane into the hydrogel by two-step crosslinking. A dry storage environment should be ensured for the hydrogel, as well as a moist hydrogel environment for the wound.

In this study, fish gelatin, collagen and $CaCO_3$ were firstly extracted from fish. Fish scale (FS)/sodium alginate/chitosan nanofibers were cross-linked with copper sulfide nanoparticles prepared by a one-step green method to obtain FS-P nanofiber hydrogels under mild conditions without catalyst and additional procedures. These fiber hydrogels not only have good tissue adhesion and tensile properties, but also have the effect of natural antibacterial and CuS photothermal synergism, which can achieve 51.32% and 49.96% of the antibacterial effect against *Staphylococcus aureus* and *Escherichia coli* respectively, avoiding the generation of superbacteria. The hydrogels transformed from nanofibers have good swelling, porosity and degradation rate. Nanofiber hydrogels are easy to store and have excellent performance in hemostasis, angiogenesis and tissue repair. This work realized the efficient utilization of marine waste and provided a new idea for the preparation of nanofiber hydrogels from marine waste.

2 Experimental

2.1 Materials

Thioacetamide (CH_3CSNH_2), acetic acid, dicyclohexyl carbon diimide (DCC), *N*,*N*-dimethylformamide (DMF) and copper nitrate ($Cu(NO_3)_2\cdot 3H_2O$) were from Aladdin. Chitosan (CS), hydrochloric acid, hydrogen peroxide solution (H_2O_2), phosphate buffered salt solution (PBS) and acetic acid were purchased from Shanghai Merck Chemical Reagent Co., Ltd, China. Sea bass and raw kelp were purchased from the Qingdao Shazikou seafood market. In addition, ultra-pure water (18.2 MΩ cm) was provided by the manufacturer. *Escherichia coli* (*E. coli*, ATCC-8739), *Staphylococcus aureus* (*S. aureus*, ATCC-14458) and human skin fibroblasts (HSF) were obtained from Qingdao University Medical College. Other reagents: DMEM (Solarbio), Phalloidin-iFluor 488 (FITC, AbCAM) and DAPI staining reagent and Matrigel matrix (Corning).

2.2 Synthesis

2.2.1 Extraction of sodium alginate. The raw kelp was soaked and treated with low dry dilute hydrochloric acid (0.01 mol L^{-1}) at 25 °C. We added sodium carbonate and reacted it at 55–75 °C for 2 h, then added water and filtered it. After 2 min, we slowly added diluted hydrochloric acid (0.02 mol L^{-1}) to the feed solution, and made it stand for 10 h, then added diluted hydrochloric acid and made it stand for 12 h. The collected substrate was dehydrated and broken, and 8% sodium carbonate was added and left for 6 h to obtain sodium alginate.

2.2.2 Extraction of fish scales. An ultrasound-assisted extraction method was used to extract collagen and $CaCO_3$. Bass scales were rinsed with distilled water (H_2O) to remove surface impurities, dried and cut into strips. Fish scales (FS) and fish glue (FG) were extracted by thermosonication, 20 mL water was added, and the fish were processed by ultrasound at 60 °C for 3 h in an ultrasonic cleaner (E15H, 37 kHz, Germany). Then acetic acid was added for acidification and decalcification, and dialysed for 36 h. The extracted fish scale solution (FS) was transferred to a 50 mL tube and freeze-dried for 72 h to obtain the upper FG solution and the lower FS solution, respectively.

2.2.3 Synthesis of CuS. In simple terms, 350 mg fish gelatin and 150 mg $Cu(NO_3)_2\cdot 3H_2O$ were dissolved in 50 mL deionized water and stirred at 1300 rpm for 20 min. 4 mL of 0.15 mol L^{-1} CH_3CSNH_2 solution was added, and the pH was adjusted to 3.5. This solution was immersed in water at 74 °C for 1 h to obtain CuS.

2.2.4 Preparation of FS-P nanofibers and FS-P hydrogels. To prepare the fibers, firstly 2 g chitosan (CS) and 0.5 g sodium alginate (SA) were dissolved in 11 g acetic acid, denoted as solution 1, and the FS solution was stirred using a magnetic mixer for 5 h, denoted as solution 2. Then the FS-P fiber membrane was prepared with electrostatic spinning equipment. The voltage was 15 kV and the flow rate of the solution was 1.5 mL h^{-1}. The distance between the needle and the receiver was about 14.2 cm. The whole spinning process was carried out at 23 °C and 36% humidity. The FS-P fiber membrane was first placed in 30 mL DMF, and 1 g DCC was added; then it was cleaned with ethanol, and finally placed in mixed fish gelatin-CuS for 12 h, dried at 70 °C in a vacuum oven, and kept at 4 °C.

2.3 Porosity and swelling rate

We tested different types of hydrogels for porosity. Freeze-dried hydrogels (W_0) and vials filled with anhydrous ethanol were weighed (W_1). The freeze-dried hydrogel was placed in vials and ultrasonically degassed to fill the hydrogel with ethanol. Then, the vial was filled with ethanol and the weight recorded (W_2). Immediately after removing the hydrogel dressing from the vial, the remaining ethanol and the vial was weighed (W_3). The formula[43] is porosity (%) = $(W_2 - W_3 - W_0)/(W_1 - W_3) \times 100\%$. We also tested different types of hydrogels for their swelling property. The dried hydrogel was initially weighed (W_0) and immersed in deionized water at room temperature until equilibrium was reached and water absorption was measured. After removing surface moisture with filter paper, the weight of the expanded sample was measured (W_t). The formula is swelling rate (%) = $[(W_t - W_0)/W_0] \times 100\%$.

2.4 Photothermal performance

In order to better demonstrate the photothermal properties of hydrogels, images of different hydrogels were recorded with irradiation at different times in our simple thermal imaging

system; the hydrogels were irradiated using a 980 nm laser (1 W cm^{-2}) for 8 min. The temperature of the membrane was recorded by infrared thermography every 30 s.

2.5 Antimicrobial activity test

The disk agar culture method was used for the antibacterial test. First, in a sterile environment, about 1×10^8 cells of *E. coli* and *S. aureus* suspensions were inoculated into a ready-to-use nutritional agar medium (9 cm × 9 cm), and the experimental materials were placed in the center of the agar medium coated with bacteria, and cultured for 20 h at a constant temperature of 32 °C. The antimicrobial effect was measured from the diameter of the inhibition of the bacteriostatic zone.

2.6 Biocompatibility of the FS-P hydrogels

In biomedical applications, the detection of biocompatibility is very necessary. Therefore, fibroblasts were seeded onto the hydrogels and their cellular responses were detected. First, the cells were co-cultured with hydrogels prepared in 24 well plates to determine whether the materials exhibited any cytotoxicity. A 24 hole plate cover was opened and placed in a glass drying tank. It was used in the experiment after being disinfected with alcohol and UV. All samples were washed with PBS and serum-free cell culture medium. Human dermal fibroblasts were inoculated into a 24 well plate with a density of 5000 cells per well. After 3 days of culture, they were taken out and fixed in 4% paraformaldehyde for 20 min. Then the cell membrane was permeated with 0.1% Triton X-100 solution for 5 min, and then washed with PBS three times. After 1% BSA solution was sealed for 1 h, PBS was washed three times. Finally, the cells were stained with 4,6-diamidino-2-phenylindole (DAPI) and fluorescein isothiocyanate phaloidin (Abcam, Shanghai, China).

2.7 Animal experiments

All experimental animal protocols were strictly carried out following the guidelines of the Animal Laboratory Supervision and Administration Committee of the Ministry of Health of the Chinese Government and associated guidelines of the Laboratory Animals Welfare Ethics Committee, and approved by the Qingdao University Laboratory Animal Welfare Ethics Committee (No. 20220123SD6620220321058).

2.7.1 Establishment of the animal models. All SD male rats were purchased from Beijing Sibefu Experimental Animal Co., Ltd, with a weight of about 0.21 kg. First, 1% pentobarbital sodium solutions were prepared, then the rats were injected intraperitoneally at a dose of 0.15 mL per 100 g. Next, hair removal cream was used to remove hair on the back of the rats. After washing, alcohol (75%) was used to disinfect the rats. After the establishment of the model, yellow fluid appeared in the rats' wound, which proved that the modeling was successful. The wound recovery was recorded.

2.7.2 Body surface animal experiments. In order to test the efficacy, 30 SD rats were randomly divided into 5 groups, with 6 rats in each group. Fiber scaffolds with appropriate shapes were cut according to the shape of skin scald wounds. Wound surfaces in each group were covered with gauze and fixed with a silk suture. The wound healing of burned rats was observed by taking photos on day 0, 3, 7 and 12 after stent covering or natural healing treatment.

2.7.3 Morphological analysis of the healing tissue. Histological staining is performed to analyze the tissue morphology of wound regeneration at different stages.[44] Hematoxylin–eosin (HE) was used to observe inflammation; Masson's trichromatic staining was used to study collagen in regenerated tissues. In brief, regenerated wound tissue collected on days 1, 3, 7, and 14 was immobilized overnight with 4% paraformaldehyde, then the tissue was embedded in paraffin and transected to a thickness of 40 μm. Hematoxylin–eosin staining and Masson's tricolor staining kit were used for tissue sections, which were analyzed, photographed and illuminated using a microscope (IX53, Olympus, Japan).

2.8 Characterization

The synthesized CuS and the composition of FS were studied by X-ray diffraction (XRD, Rigaku). Then, the synthesis of PS-P hydrogel was verified by FTIR spectroscopy using a Bruker second-generation D2 instrument with 30 mA and 30 keV operating current and voltage, respectively, and an FT-IR instrument (PerkinElmer, Spectrum 2000) with wavenumber in the range of 4000–400 cm^{-1} and operating frequency of 75.5 MHz. A scanning electron microscope (SEM, Micrion FEI PHILIPS) was used to observe the morphology. The network elements were analyzed by energy dispersive spectroscopy (EDS). The rheological test was performed using an Anton Pa MCR92 rheometer. The photothermal effect was studied using a self-made thermal imaging system consisting of an infrared thermal imager (Kalibrierschein 3825/2015, JENOPTIK) and an optical digital camera.

3 Results and discussion

3.1 Synthesis of FS-P nanofiber hydrogels

The nanofiber hydrogels were obtained from a marine ecosystem (Scheme 1). Fish scales come from sea bass which is the main cultured marine fish species in China. Fish scales of sea bass are generally regarded as inedible waste. Therefore, sea bass scales were selected as representative scales for collagen extraction. Fig. S1† shows the flow chart of extracting collagen and $CaCO_3$ solution from fish scales. They undergo a series of treatments to get the upper and lower fluids, which are used to make the raw material for the nanofibers. Fig. 1A shows the preparation process of the fiber hydrogel. First, CuS nanoparticles (Fig. S2 and S3A†) were prepared in one step in fish glue, in which $Cu(NO_3)_2$, CH_3CSNH_2 and fish gelatin were stored at 78 °C for 56 min. The prepared copper sulfide nanoparticles have a diameter of about 10 nm and have good dispersibility. Compared with copper sulfide in previous studies requiring multi-step or high-pressure conditions, the proposed one-step green method has more advantages, especially in saving time and increasing yield. Fig. 1B shows the XRD curve of FS, and it could be seen that the vibration was obvious at 10.32°,

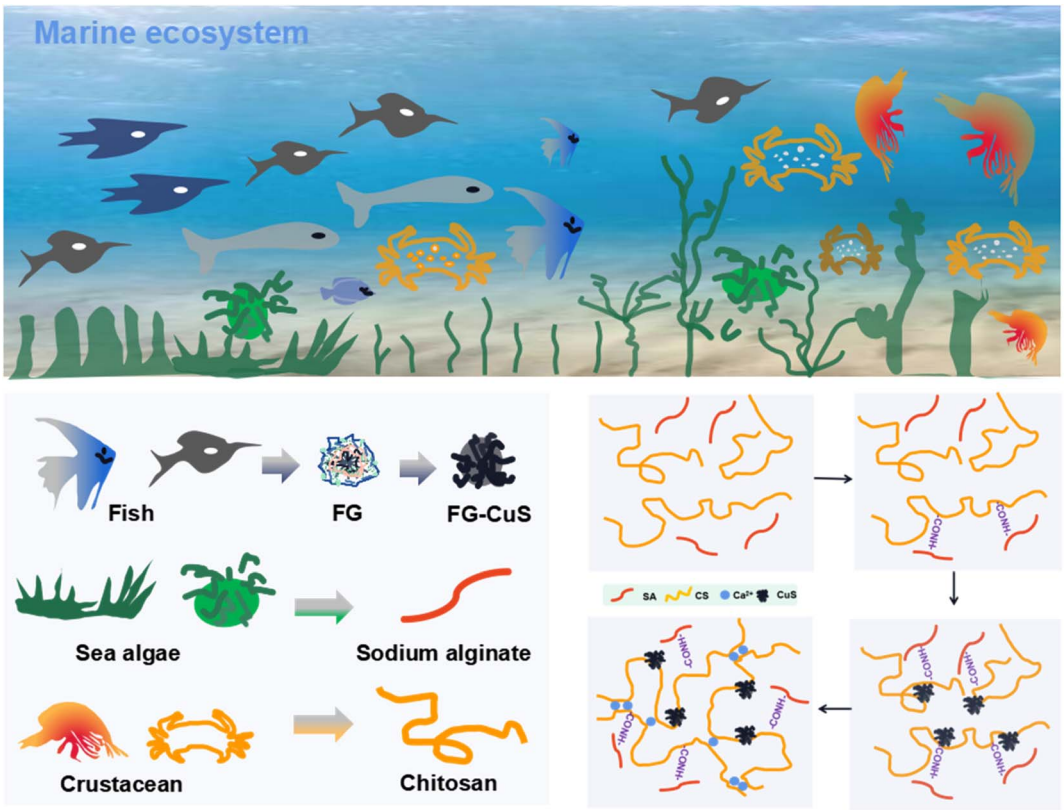

Scheme 1 Fish scale/sodium alginate/chitosan nanofiber hydrogels based on a marine ecosystem.

17.96° and 24.46°, which proved that the FS contains $CaCO_3$ and other forms of Ca.

Secondly, FS-P nanofibers were prepared by electrostatic spinning. The FTIR spectra obtained showed that the fibers were composed of FS, sodium alginate and chitosan (Fig. 1C). The vibration peak of COO from FS and sodium alginate could be seen at 1400 cm^{-1}, and the vibration peak of NH_3 from chitosan could be seen at 1590 cm^{-1}. Then the FS-P nanofibers were immersed in the synthetic FG-CuS to prepare the FS-P hydrogel. As shown in Fig. S3B,† CuS was used for FS-P nanofibers and produced cross-linking, where Ca^{2+} and sodium alginate generated the cross-linking. As shown in the FS-P hydrogel curve in the FTIR spectrum, the CONH bond was generated at 1690 cm^{-1}, indicating further cross-linking between SA, collagen and chitosan. Moreover, there was a weak amide peak at 2980 cm^{-1}, indicating that there were some proteins, which verified the successful extraction of collagen above. Considering that these proteins were derived from fish gelatin (FG) during the synthesis of CuS, this result also proved the existence of CuS from another angle. More notably, it could be seen from Fig. 1D that the fiber diameter distribution was uniform with pore size distribution, while FS-P hydrogel soaked in FG-CuS also had uniform pore size distribution after freeze-drying, which endowed the fiber hydrogel with water absorption and retention characteristics. However, the FS-P prepared without spinning did not have such a structure (Fig. S4†).

3.2 Morphology and properties of the hydrogels

The FS-P hydrogel was obtained by regulating the cross-linked FS-P fiber through CuS, because we accidentally found that it was not only related to the concentration of CuS, but also to the diameter of the fiber. Three fibers of uniform diameter and concentration were set up for the study. Fig. 1A shows the SEM image and DES surface scan image of FS-P-2. It can be seen that there are many pore sizes, and it is obvious that the O element comes from macromolecules such as collagen, chitosan and sodium alginate. Ca element is derived from $CaCO_3$ in fish scales, while Cu and S elements are derived from FG-CuS. CuS was successfully extracted and synthesized from fish scale solution, and CuS was introduced into the hydrogel. As shown in Fig. S5,† the pore size distribution of fiber hydrogels obtained for FS-P-1 and FS-P-3 fiber membranes was poor. In order to study the causes, rheological shear tests were carried out (Fig. 2B), and FS-P-2 hydrogels showed stable moduli compared with FS-P-1 and FS-P-3 hydrogels, which may be one of the reasons for the difference in SEM morphology. Porosity statistics were conducted (Fig. 2C) and it was found that the porosity of FS-P-2 hydrogel was greater than that of FS-P-1 and FS-P-3 hydrogels, which resulted in the difference in swelling capacity. Fig. 2D shows the swelling rate statistics over time, FS-P-2 hydrogel has the highest swelling rate. However, considering that medical excipients should have good compressive and cutting resistance, compression cutting and adhesion tests were carried out. Fig. S6† shows that it can remain intact after

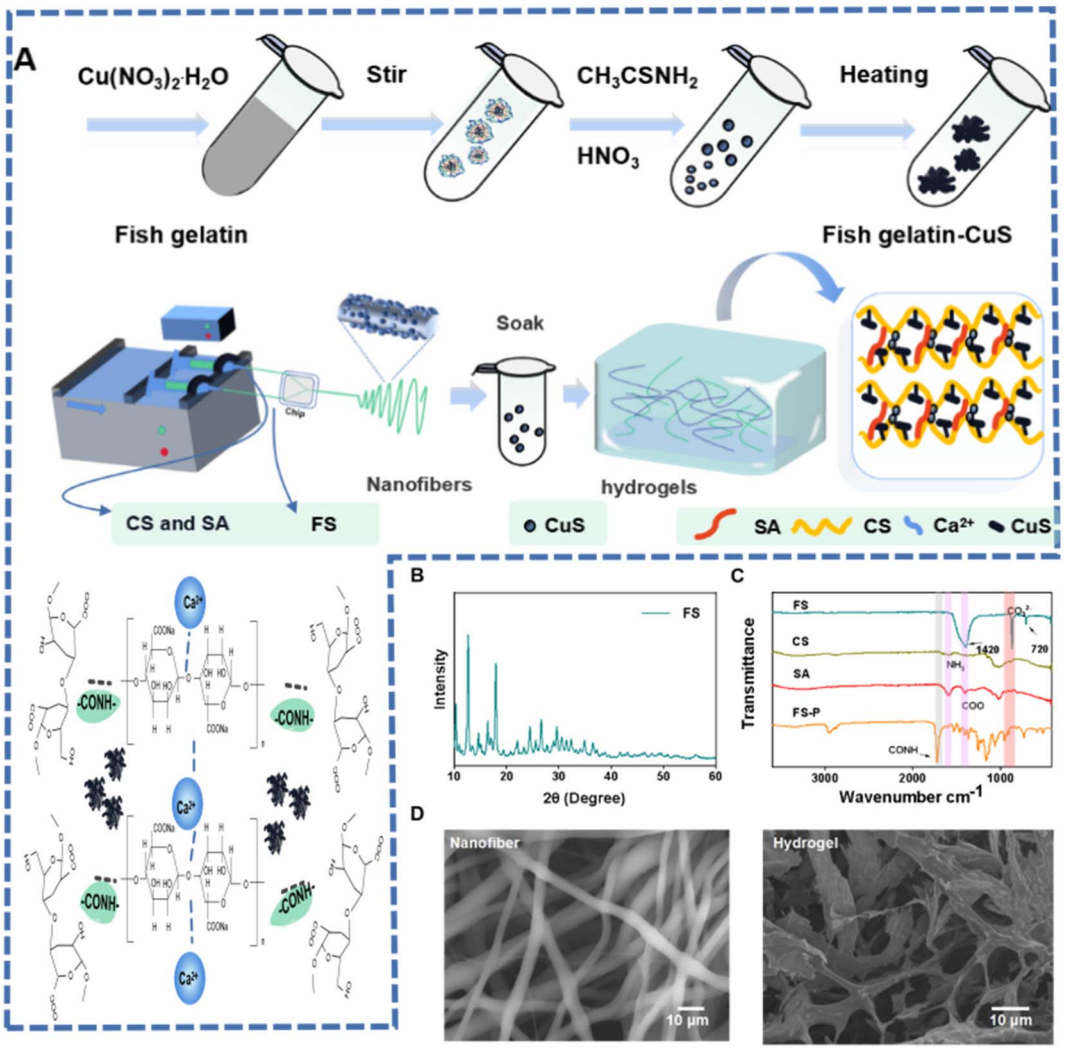

Fig. 1 (A) Synthesis schematic diagram of FS-P hydrogel. (B) X-ray diffraction (XRD) pattern. (C) FT-IR spectra. (D) SEM images of FS-P nanofibers and FS-P hydrogel.

heavy compression and knife cutting. Medical excipients must have a certain adhesion to satisfy the filling of geometric tissue. Natural macromolecule CS and collagen have good adhesion to the FS-P fiber hydrogel due to their active groups such as amino, carboxyl and hydroxyl groups (Fig. S7†), especially to the skin of animal tissues. Fig. S8† shows the shear stretch curve of hydrogel adhesion to pig skin. It can be seen that hydrogels can withstand stresses of 0.23 MPa. Finally, FS-P-1, FS-P-2 and FS-P-3 hydrogels all degraded about 40% within 14 days. In conclusion, marine waste-based FS-P-2 nanofiber hydrogels have great advantages as tissue repair materials for medical purposes.

3.3 Photothermal test and *in vitro* antibacterial activity test

CuS has good photothermal conversion performance, so the antibacterial properties of CS, and $CaCO_3$ of FS-P are combined with the photothermal antibacterial properties of CuS. So we first verified the photothermal effect. Fig. 3A shows the infrared thermal imaging image of FS-P hydrogel irradiated at 980 nm. It can be seen that the temperature of FS-P hydrogel gradually rises with time. However, with the increase of time, the heating rate gradually slows down and does not continue to rise after a certain temperature is reached, while about 55 °C is enough to kill bacteria and other pathogens without harming its own tissues and cells (Fig. 3B). The bactericidal effect of the fiber hydrogel on Gram-negative bacteria and Gram-positive bacteria was tested before the tissue repair effect was verified. In the following experiment, under irradiation, *in vitro* antibacterial experiments were carried out. *Escherichia coli* (*E. coli*) and *Staphylococcus aureus* (*S. aureus*) were selected and evaluated *in vitro* by the disk agar culture method. Firstly, there was no obvious antibacterial ring in the CS group, but when the membrane was uncovered, there was no *Staphylococcus aureus* under the membrane (Fig. S9†). The most probable reason is that CS itself has good antibacterial activity, and there is no antibacterial ring because the CS can't spread out. The FS-P group had no obvious antibacterial effect, because the diffusivity of fibers led to a poor diffusion effect and no large antibacterial ring, which prevented good inhibition of the

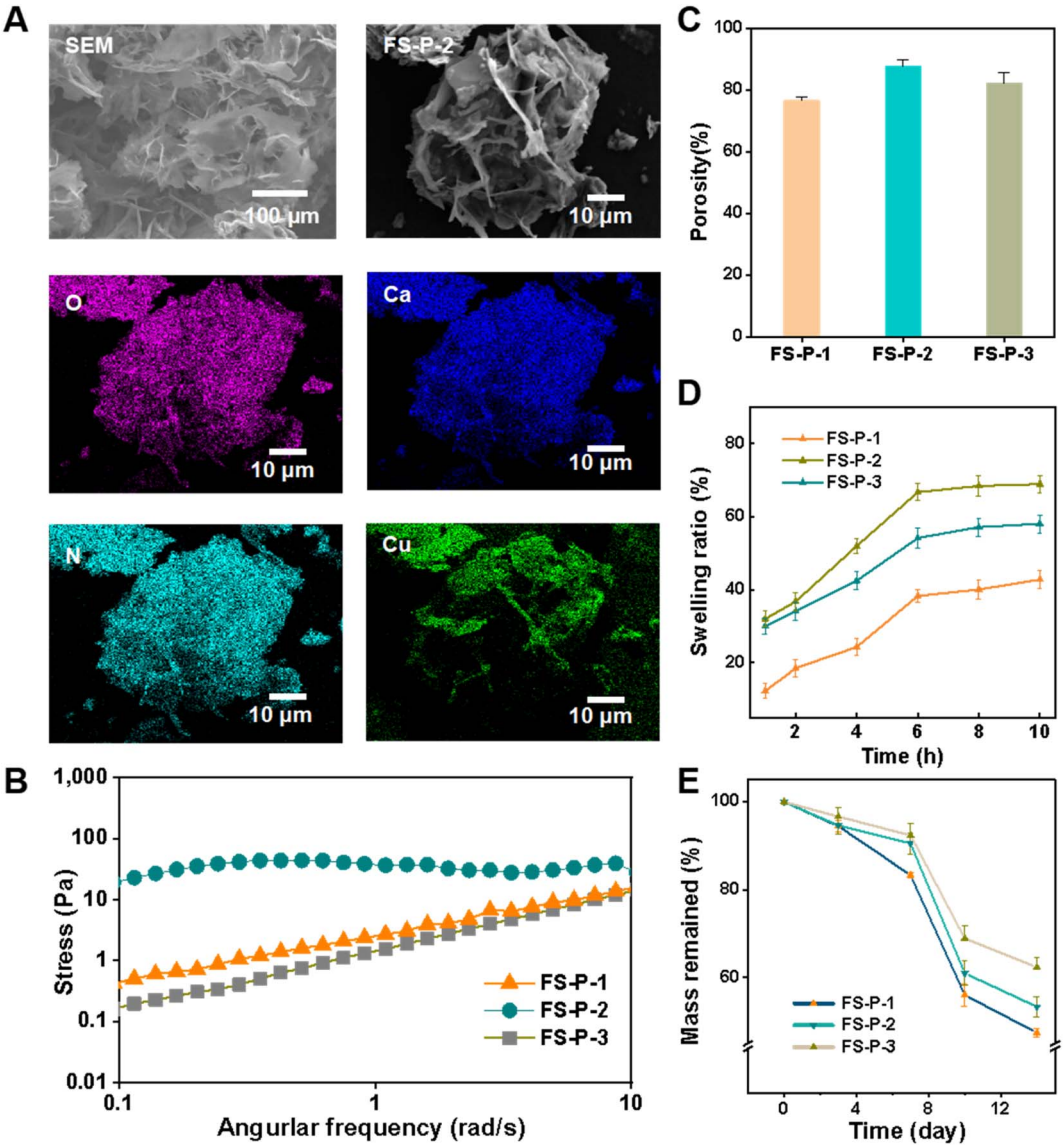

Fig. 2 (A) SEM images and EDS of FS-P hydrogel. (B) Shear rheological curves of FS-P at different concentrations. (C) Swelling rate statistics. (D) Curve of swelling rate over time and (E) degradation over time of FS-P hydrogel at different concentrations.

colonization and growth of surrounding bacteria. However, the FS-P hydrogel group soaked in FG-CuS produced larger bacteriostatic zones for *S. aureus* and *E. coli* compared with the FS-P group, because the FS-P hydrogels released calcium ions which could make it spread around to kill bacterial pathogens (Fig. 3C). Statistical analysis (Fig. 3D) showed that the antibacterial effect of the FS-P hydrogel group against *S. aureus* and *E. coli* could reach 51.32% and 49.96%. Further SEM images of *E. coli* and *S. aureus* (Fig. 3E and F) confirm that the initial *E. coli* show a rod-like structure, smooth surface and complete morphology without cell breakage. After treatment with FS-P hydrogel, the bacterial cell membrane was wrinkled and constricted on the surface of the cell membrane without fullness (Fig. 3E). *S. aureus* presented similar results to *E. coli* (Fig. 4F). All these results can confirm that the photothermal antibacterial properties of CuS and the interaction between chitosan and calcium carbonate in fish scales and microbial cell membranes lead to the leakage of bacterial proteins and other cellular components, resulting in antimicrobial effects. That is sufficient to play an antibacterial role in the early stage of tissue repair and provide the first layer of guarantee for tissue repair.

3.4 Biocompatibility

For *in vivo* application, nanofilm hydrogels were not required to be cytotoxic, so human fibroblasts were transplanted onto the FS-P nanofiber membrane and FS-P hydrogels to evaluate their cellular responses. As a positive control, polystyrene tissue culture plates (TCP) were used to culture fibroblasts on the same day as controls. The adhesion and morphology of human fibroblasts were detected by an actin cytoskeleton and nuclear double-labeled fluorescence staining. Fig. 4A shows that the three fiber membranes and the cells on TCP have similar

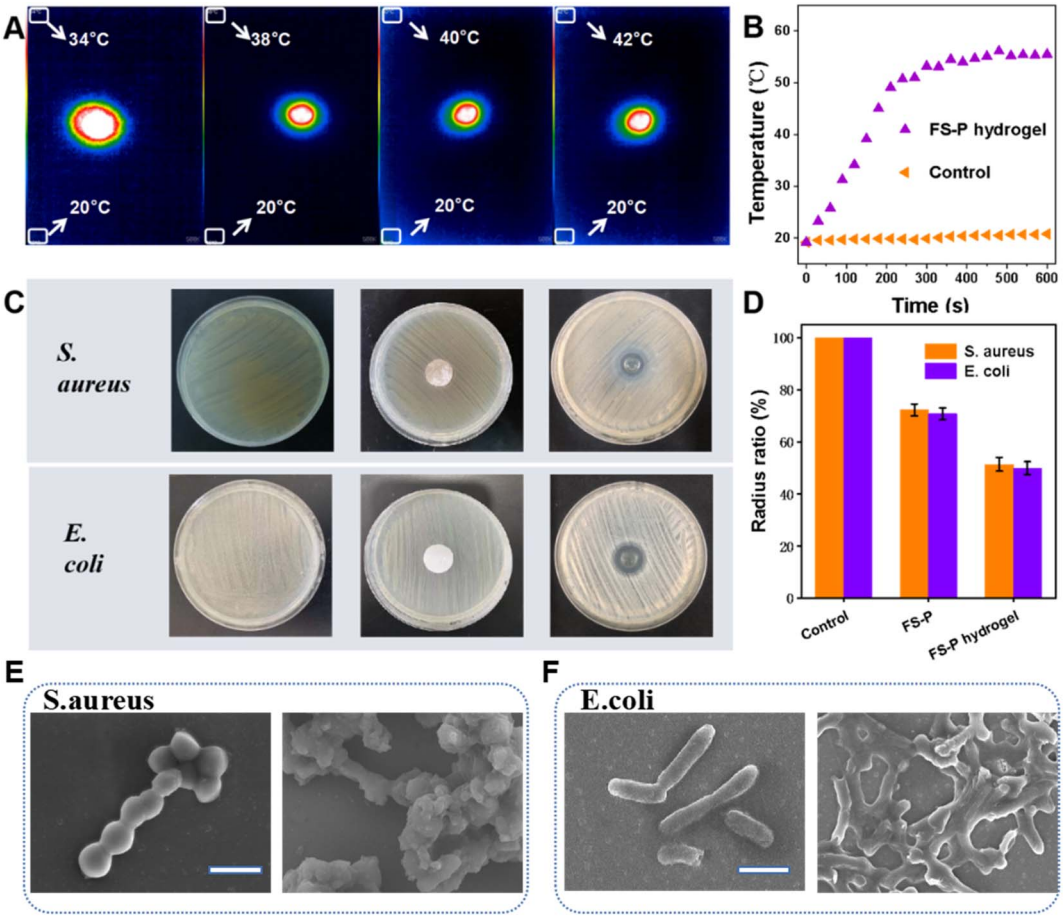

Fig. 3 (A) Thermal images of FS-P hydrogels irradiated at 980 nm, and (B) heating curves of FS-P hydrogels irradiated at 980 nm. (C) Growth of *S. aureus* and *E. coli* after 24 h incubation on an agar plate. (D) Bacterial survival rate of *S. aureus* and *E. coli*. (E) SEM images of *S. aureus* before and after treatment with FS-P hydrogel (scale bar: 200 nm). (F) SEM images of *E.coli* before and after treatment with FS-P hydrogel (scale bar: 200 nm).

fusiform morphology. It can be seen that the cell morphologies of the FS-P nanofiber membrane and the FS-P hydrogel group and the control group are basically the same. Quantitative statistics of CCK-8 (Fig. 4B) showed that there was no significant difference between the fiber membrane and TCP, and the cells could still survive, and the OD value of the FS-P hydrogel group was significantly higher than that of the control group, with a significant difference (**$P < 0.01$). All in all, this indicates that the FS-P nanofiber membrane and FS-P hydrogel have almost no cytotoxic effect, and FS-P hydrogel can also promote cell proliferation, which may be because the microscopic microenvironment of the hydrogel (Fig. 1E) provides a better migration

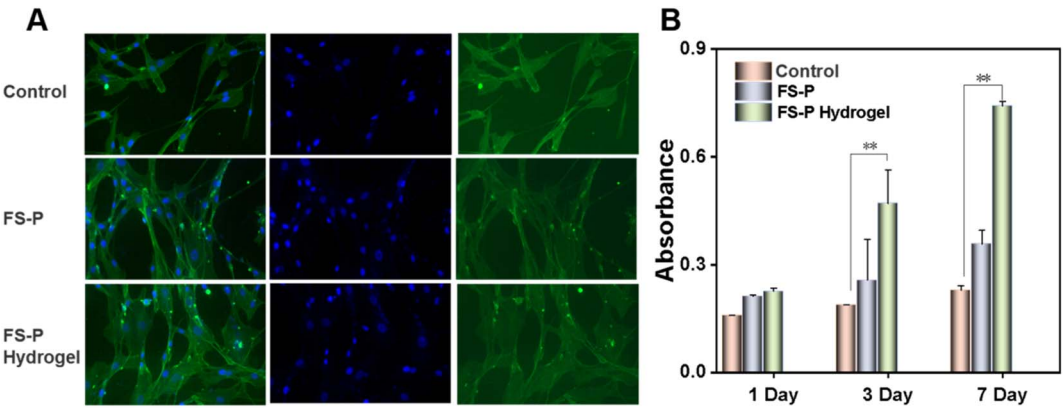

Fig. 4 (A) Images of FITC-Photolipin and DAPI dual staining of human fibroblasts cultured on day 3. (B) Statistics of CCK-8 values measured by direct contact between different materials and cells ($n = 6$, ***$p < 0.001$, **$p < 0.01$, *$p < 0.05$).

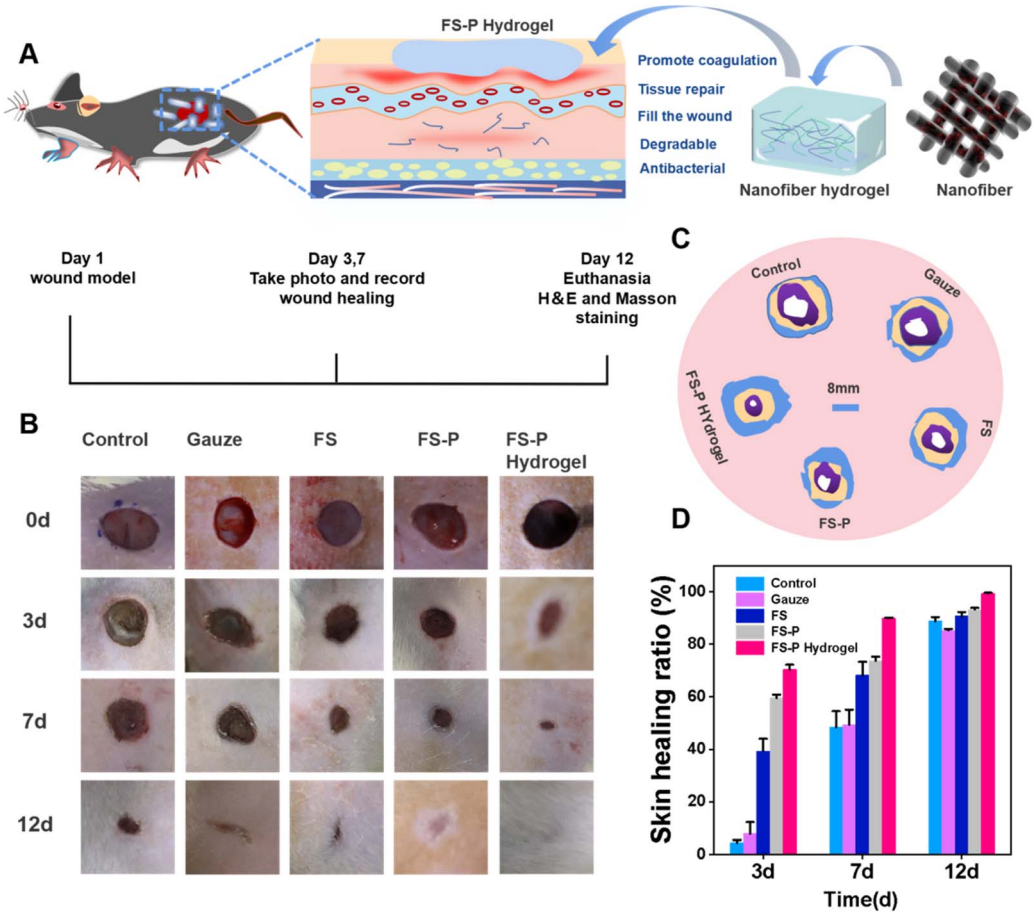

Fig. 5 (A) Diagram of the tissue repair mechanism of FS-P hydrogel. (B) Photographs of the wound recovery process with different material treatments. (C) Schematic representation of the comparison of wound healing with different materials. (D) Wound healing rate statistics.

and proliferation effect, and has a certain promoting effect on cell growth. The applicability of FS-P hydrogel as a waste material to explore its biomedical applications was emphasized.

3.5 Animal experiment

In the traditional electrostatic spinning method to prepare the fiber membrane, the nanofibers produced are basically secondary bonding in the wound; the adhesion between the fiber membrane and the wound is relatively poor, and cannot match the geometry of the wound structure. Fig. S10† shows that the traditional fiber membrane and nanofiber hydrogels covered the skin. Adhesion between the fiber membrane and the skin was weak; however, FS-P nanofiber hydrogels had a good adhesion effect, and better adhesion may have an impact on repair. Therefore, based on FS-P nanofibers and FS-P nanofiber hydrogels, the effects of spinning methods and different adhesion of fiber hydrogels on tissue repair were further compared.

Over the next few days, we evaluated wound recovery in 30 male rats. Each group ate and drank normally during the experiment, and were normally and actively responsive to sound stimuli. No symptoms of diarrhea, allergy or abnormal body temperature were observed (Fig. S11†). An infected wound was established on the back as shown in Fig. 4A. With the aim of better fixing the FS-P fiber hydrogel on the wound, a rubber pad was sewn on the infected site of rats. The wound surface was photographed on the 1st, 3rd, 7th, and 12th days and then the effects of different subsequent treatment methods on the recovery were respectively observed and recorded on the 1st, 3rd, 7th, and 12th days. As shown in Fig. 5B, the wound recovery rate of the control group and the gauze group was slower, wound suppuration occurred on the 3rd day, and the wound did not heal after 12 days, with a large scab. The FS group and the FS-P group had significantly less pus on the 3rd day, because of the weak antibacterial effect (Fig. 5C). On the 12th day, the scab of the FS group and FS-P group was smaller than that of the first two groups, because FS and FS-P groups had good biocompatibility, and could also protect the wound, isolate contamination and avoid wound infection. On the 12th day, the skin structure of the SD rats in the FS-P hydrogel group was clear and the epidermis was completely covered, which was due to the ability of FS-P hydrogel to promote cell growth and effectively accelerate wound healing. Fig. 5C shows the area simulation of the infection window in rats. It can be seen that the area of the FS-P hydrogel group changed fastest, which vividly demonstrates the repair ability of the hydrogel. It can even be seen from Fig. 5D

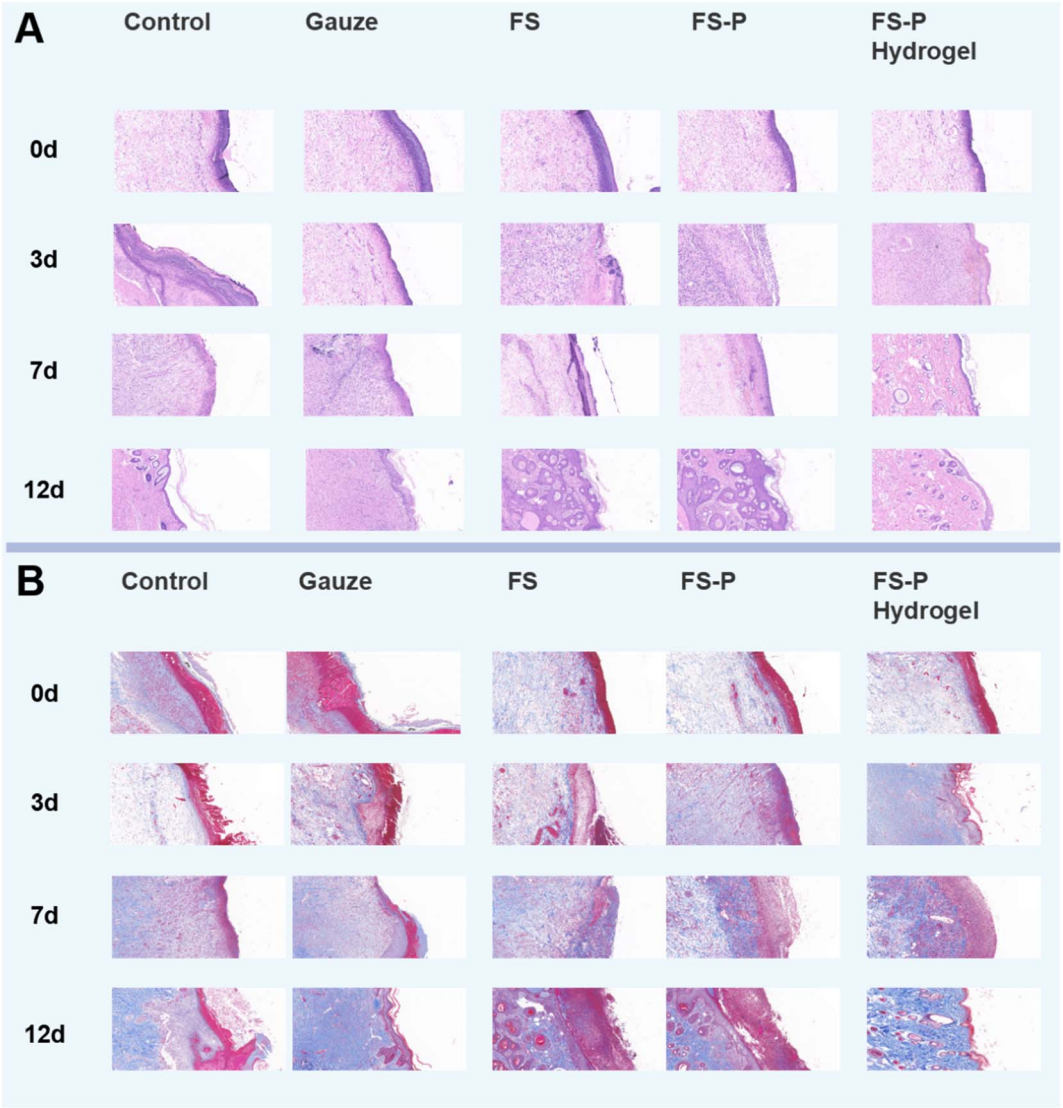

Fig. 6 HE (A) and Masson (B) staining images of wound treated in different ways; the bar represents 200 μm.

that the FS-P hydrogel group had the highest repair rate, reaching 99.36%. This may be due not only to the antibacterial ability of CuS with CS and $CaCO_3$ but also to the growth-promoting ability of FS-P hydrogel. While repairing wound tissue, it can effectively reduce bacterial infection and accelerate wound healing. The advantages of FS-P nanofiber hydrogel extracted from marine waste as scaffold materials for biomedical applications were verified.

3.6 Histological analysis

There are complex processes in tissue repair. To further study the relation between infection and recovery in tissue repair, histopathological examinations were performed on the 1st, 3rd, 7th, and 12th days for tissues treated in different ways. It can be seen from Fig. 6A that there were more lymphocytes in the control and gauze groups on the 3rd day of infection, while in the FS group they were relatively less, indicating that the FS group could protect the wound from bacterial infection due to the coverage of the fiber membrane. On the 7th day, there were fewer lymphocytes in the FS-P group than in the first three groups, due to the antibacterial effects of CS and FS themselves, which can dissolve bacteria and thus reduce bacteria at the wound site. On the 12th day, the blood vessels in the FS-P hydrogel group were significantly more than those in the FS-P group, because the photothermal effect of CuS not only enhanced the antibacterial effect (Fig. S12†), but also promoted the growth of FS-P hydrogel, which was conducive to cell attachment. This proves that the use of fiber hydrogel can further improve the effectiveness of antibacterial activity and repair.

Masson staining was used to observe collagen deposition in wound tissue (Fig. 6B). It can be seen that on the 3rd day, in the control group, a few collagen fibers appeared; the same was true for the gauze group and FS group. On the 7th day, collagen fibers and blood vessels in the FS-P group and the FS-P hydrogel group began to increase compared with the first three groups

(Fig. S13A†). On the 14th day, the gauze group and FS group blue collagen fiber and granulation tissue number was lower, the FS-P hydrogel group collagen fibers were more dense, first forming a complete layer of epithelial tissue, indicating that tissue repair was completed (Fig. S13B†). These experimental results indicated that antibacterial therapy alone in the early stage was not sufficient for wound repair. But also in reduced inflammation, at the same time promoted wound healing. The results confirmed the significance of FS-P hydrogel in wound repair.

4 Conclusion

In this study, collagen and other molecular substances were extracted from fish. CuS nanoparticles prepared by a one-step green method were combined with FS-P nanofibers. Under mild conditions, the FS-P nanofiber hydrogels were obtained by *in situ* cross-linking of nanofibers without catalyst and additional steps. This fiber hydrogel not only has good tissue adhesion and tensile properties, but also has the effect of natural antibacterial and CuS photothermal synergism, the antibacterial effect of the FS-P hydrogel group against *S. aureus* and *E. coli* could reach 51.32% and 49.96%, respectively. The FS-P nanofiber hydrogel has 87.56% voidage and 52.68% degradability after 14 days. It also has multiple functions of promoting cell proliferation, angiogenesis and tissue repair. The comprehensive strategy of using this marine bio-based raw material and using fibers as a precursor to prepare a gel provides new insights into the FS-P scaffold for wound dressing.

Conflicts of interest

There are no conflicts to declare.

Acknowledgements

This work was supported by the National Natural Science Foundation of China (11904193 and 51973100) and the State Key Laboratory of Bio-Fibers and Eco-Textiles, Qingdao University (RZ2000003334 and G2RC202022).

References

1 M. M. Islam and R. Chuenpagdee, Towards a classification of vulnerability of small-scale fisheries, *Environ. Sci. Policy*, 2022, **134**, 1–12.
2 M. Miya, Environmental DNA Metabarcoding: A Novel Method for Biodiversity Monitoring of Marine Fish Communities, *Ann. Rev. Mar. Sci*, 2022, **14**, 161–185.
3 A. R. Watson, C. Blount, D. P. Mcphee, *et al.*, Source, fate and management of recreational fishing marine debris, *Mar. Pollut. Bull.*, 2022, **178**, 113500.
4 N. Pacoureau, C. L. Rigby, P. M. Kyne, *et al.*, Half a century of global decline in oceanic sharks and rays, *Nature*, 2021, **589**(7843), 567–571.
5 L.-X. Zheng, X.-Q. Chen and K.-L. Cheong, Current trends in marine algae polysaccharides: The digestive tract, microbial catabolism, and prebiotic potential, *Int. J. Biol. Macromol.*, 2020, **151**, 344–354.
6 W. Levasseur, P. Perre and V. Pozzobon, A review of high value-added molecules production by microalgae in light of the classification, *Biotechnol. Adv.*, 2020, **41**, 107545.
7 J. R. Griffiths, M. Kadin, F. J. A. Nascimento, *et al.*, The importance of benthic-pelagic coupling for marine ecosystem functioning in a changing world, *Global Change Biol.*, 2017, **23**(6), 2179–2196.
8 O. Felfoul, M. Mohammadi, S. Taherkhani, *et al.*, Magneto-aerotactic bacteria deliver drug-containing nanoliposomes to tumour hypoxic regions, *Nat. Nanotechnol.*, 2016, **11**(11), 941–947.
9 S. U. Kadam, B. K. Tiwari and C. P. O'donnell, Extraction, structure and biofunctional activities of laminarin from brown algae, *Int. J. Food Sci. Technol.*, 2015, **50**(1), 24–31.
10 M. Wang, L. Chen and Z. Zhang, Potential applications of alginate oligosaccharides for biomedicine-A mini review, *Carbohydr. Polym.*, 2021, **271**, 118408.
11 Saraswati, P. E. Giriwono, D. Iskandriati, *et al.*, Screening of In-Vitro Anti-Inflammatory and Antioxidant Activity of Sargassum ilicifolium Crude Lipid Extracts from Different Coastal Areas in Indonesia, *Mar. Drugs*, 2021, **19**(5), 252.
12 B.-R. Chen, C.-L. Gao, J. Liu, *et al.*, Diversity-oriented synthesis of marine sponge derived hyrtioreticulins and their anti-inflammatory activities, *Chin. J. Nat. Med.*, 2022, **20**(1), 74–80.
13 Z. Wei, J. H. Yang, Z. Q. Liu, *et al.*, Novel Biocompatible Polysaccharide-Based Self-Healing Hydrogel, *Adv. Funct. Mater.*, 2015, **25**(9), 1352–1359.
14 Y. Yuan, Q. Yu, M. Cao, *et al.*, Selective extraction of uranium from seawater with biofouling-resistant polymeric peptide, *Nat. Sustainability*, 2021, **4**(8), 708–714.
15 S. I. Faria, R. Teixeira-Santos, M. J. Romeu, *et al.*, Unveiling the Antifouling Performance of Different Marine Surfaces and Their Effect on the Development and Structure of Cyanobacterial Biofilms, *Microorganisms*, 2021, **9**(5), 1102.
16 D. N. Carvalho, R. Lopez-Cebral, R. O. Sousa, *et al.*, Marine collagen-chitosan-fucoidan cryogels as cell-laden biocomposites envisaging tissue engineering, *Biomed. Mater.*, 2020, **15**(5), 055030.
17 T. Abudula, T. Colombani, T. Alade, *et al.*, Injectable Lignin-co-Gelatin Cryogels with Antioxidant and Antibacterial Properties for Biomedical Applications, *Biomacromolecules*, 2021, **22**(10), 4110–4121.
18 Z.-K. Cui, S. Kim, J. J. Baljon, *et al.*, Microporous methacrylated glycol chitosan-montmorillonite nanocomposite hydrogel for bone tissue engineering, *Nat. Commun.*, 2019, **10**, 3523.
19 M. A. Darabi, A. Khosrozadeh, R. Mbeleck, *et al.*, Skin-Inspired Multifunctional Autonomic-Intrinsic Conductive Self-Healing Hydrogels with Pressure Sensitivity, Stretchability, and 3D Printability, *Adv. Mater.*, 2017, **29**(31), DOI: 10.1002/adma.201700533.
20 Y. Liang, Z. Li, Y. Huang, *et al.*, Dual-Dynamic-Bond Cross-Linked Antibacterial Adhesive Hydrogel Sealants with On-

Demand Removability for Post-Wound-Closure and Infected Wound Healing, *ACS Nano*, 2021, **15**(4), 7078–7093.

21 B. Qu and Y. Luo, Chitosan-based hydrogel beads: Preparations, modifications and applications in food and agriculture sectors - A review, *Int. J. Biol. Macromol.*, 2020, **152**, 437–448.

22 L. Sheng, Z. Zhang, Y. Zhang, *et al.*, A novel "hot spring"-mimetic hydrogel with excellent angiogenic properties for chronic wound healing, *Biomaterials*, 2021, **264**, 120414.

23 B. Zhang, J. He, M. Shi, *et al.*, Injectable self-healing supramolecular hydrogels with conductivity and photo-thermal antibacterial activity to enhance complete skin regeneration, *Chem. Eng. J.*, 2020, **400**, 125994.

24 Y. Yang, X. Wang, F. Yang, *et al.*, Highly Elastic and Ultratough Hybrid Ionic-Covalent Hydrogels with Tunable Structures and Mechanics, *Adv. Mater.*, 2018, **30**(18), 1707071.

25 X. Zhao, H. Wu, B. Guo, *et al.*, Antibacterial anti-oxidant electroactive injectable hydrogel as self-healing wound dressing with hemostasis and adhesiveness for cutaneous wound healing, *Biomaterials*, 2017, **122**, 34–47.

26 T. M. Wilkinson, C. K. F. Li, C. S. C. Chui, *et al.*, Preexisting influenza-specific CD4(+) T cells correlate with disease protection against influenza challenge in humans, *Nat. Med.*, 2012, **18**(2), 274–280.

27 M. Azizi, R. E. Schmieder, F. Mahfoud, *et al.*, Endovascular ultrasound renal denervation to treat hypertension (RADIANCE-HTN SOLO): a multicentre, international, single-blind, randomised, sham-controlled trial, *Lancet*, 2018, **391**(10137), 2335–2345.

28 X. Liu, Y. Yang, D.-G. Yu, *et al.*, Tunable zero-order drug delivery systems created by modified triaxial electrospinning, *Chem. Eng. J.*, 2019, **356**, 886–894.

29 N. Xu, X.-L. Peng, H.-R. Li, *et al.*, Marine-Derived Collagen as Biomaterials for Human Health, *Front. Nutr.*, 2021, **8**, 702108.

30 H. Qiao, T. Guo, Y. Zheng, *et al.*, A novel microporous oxidized bacterial cellulose/arginine composite and its effect on behavior of fibroblast/endothelial cell, *Carbohydr. Polym.*, 2018, **184**, 323–332.

31 Y. Zhao, B. Zhu, Y. Wang, *et al.*, Effect of different sterilization methods on the properties of commercial biodegradable polyesters for single-use, disposable medical devices, *Mater. Sci. Eng., C*, 2019, **105**, 110041.

32 A. C. Mendes, K. Stephansen and I. S. Chronakis, Electrospinning of food proteins and polysaccharides, *Food Hydrocolloids*, 2017, **68**, 53–68.

33 L. F. Boesel, R. L. Reis and J. S. Roman, Innovative Approach for Producing Injectable, Biodegradable Materials Using Chitooligosaccharides and Green Chemistry, *Biomacromolecules*, 2009, **10**(3), 465–470.

34 J. Xu, G. M. Soliman, J. Barralet, *et al.*, Mollusk Glue Inspired Mucoadhesives for Biomedical Applications, *Langmuir*, 2012, **28**(39), 14010–14017.

35 P. Manivasagan, S. Bharathiraja, M. S. Moorthy, *et al.*, Marine Biopolymer-Based Nanomaterials as a Novel Platform for Theranostic Applications, *Polym. Rev.*, 2017, **57**(4), 631–667.

36 M. Shi, H. Zhang, T. Song, *et al.*, Sustainable Dual Release of Antibiotic and Growth Factor from pH-Responsive Uniform Alginate Composite Microparticles to Enhance Wound Healing, *ACS Appl. Mater. Interfaces*, 2019, **11**(25), 22730–22744.

37 Y. Liang, Y. Liang, H. Zhang, *et al.*, Antibacterial biomaterials for skin wound dressing, *Asian J. Pharm. Sci.*, 2022, **17**(3), 353–384.

38 Y. Liang, M. Li, Y. Yang, *et al.*, pH/Glucose Dual Responsive Metformin Release Hydrogel Dressings with Adhesion and Self-Healing *via* Dual-Dynamic Bonding for Athletic Diabetic Foot Wound Healing, *ACS Nano*, 2022, **16**(2), 3194–3207.

39 Y. Huang, L. Mu, X. Zhao, *et al.*, Bacterial Growth-Induced Tobramycin Smart Release Self-Healing Hydrogel for Pseudomonas aeruginosa-Infected Burn Wound Healing, *ACS Nano*, 2022, **16**(8), 13022–13036.

40 J. H. Cho, J. S. Lee, J. Shin, *et al.*, Ascidian-Inspired Fast-Forming Hydrogel System for Versatile Biomedical Applications: Pyrogallol Chemistry for Dual Modes of Crosslinking Mechanism, *Adv. Funct. Mater.*, 2018, **28**(6), 1705244.

41 J. Zhou, W. Liu, X. Zhao, *et al.*, Natural Melanin/Alginate Hydrogels Achieve Cardiac Repair through ROS Scavenging and Macrophage Polarization, *Adv. Sci.*, 2021, **8**(20), 2100505.

42 D. J. Schupp, X. Zhang, S. Sun, *et al.*, Mineral plastic hydrogels from the cross-linking of polyacrylic acid and alkaline earth or transition metal ions, *Chem. Commun.*, 2019, **55**(34), 4913–4916.

43 Z. Fan, B. Liu, J. Wang, *et al.*, A Novel Wound Dressing Based on Ag/Graphene Polymer Hydrogel: Effectively Kill Bacteria and Accelerate Wound Healing, *Adv. Funct. Mater.*, 2014, **24**(25), 3933–3943.

44 M. Zhao, Z. Tang, X. Zhang, *et al.*, A self-healing, stretchable, and conductive Poly(N-vinylpyrrolidone)/gallic acid composite hydrogel formed *via* hydrogen bonding for wearable electronic sensors, *Compos. Sci. Technol.*, 2020, **198**, 108294.